Wind-Optimal Trajectories for Multirotor eVTOL Aircraft on UAM Missions

Priyank Pradeep *, Gano B. Chatterji †, Banavar Sridhar ‡, Kaj-Martin Edholm §
NASA Academic Mission Services, NASA Ames Research Center, Moffett Field, CA, 94035, USA.

Todd A. Lauderdale ¶, Kapil Sheth ‖, Chok Fung Lai **, Heinz Erzberger ††
NASA Ames Research Center, Moffett Field, CA, 94035, USA.

Distributed electric propulsion powered electric vertical takeoff and landing aircraft are expected to enable urban air mobility. Low specific energy of onboard lithium-ion polymer batteries and wind conditions impose constraints on flight endurance. Therefore, from the safety and efficiency perspective, planning and flying minimum energy trajectories are important. The primary motivation for this paper is to determine if there is an operational benefit to flying wind-optimal trajectories for short flights (less than 60 miles) in the urban environment. This study employs wind-optimal trajectories for a NASA-proposed conceptual multirotor aircraft flight in the urban environment. The optimal control model presented includes a wind model for quantifying the effect of wind on the trajectory. The optimal control problem is numerically solved using the direct method. Energy consumption and flight duration flying wind-optimal trajectories between origins and destinations in a metropolitan area are compared with energy consumption and flight duration flying on the great-circle paths between the same origin and destination pairs to determine the operational benefit of wind-optimal routing for short flights. The flight duration results for different scenarios are validated using a simulation tool designed and developed by NASA for exploring advanced air traffic management concepts. In summary, this research study suggests that for short flights in an urban environment, the wind-optimal trajectories have a very slight (insignificant) operational advantage over the great-circle trajectories in terms of energy consumption and flight duration. As expected, headwinds and tailwinds along the route of flight have a significant impact on energy consumption and flight duration.

I. Nomenclature

D	=	Parasite drag
T	=	Net thrust
T_{rotor}	=	Thrust produced by an isolated rotor
λ	=	Latitude of the eVTOL aircraft
τ	=	Longitude of the eVTOL aircraft
h	=	Altitude above mean sea level of the eVTOL aircraft
v_h	=	Rotor induced velocity in hover
v_i	=	Rotor induced velocity during forward flight
V	=	True airspeed of the eVTOL aircraft
V_{GS}	=	Ground speed of the eVTOL aircraft
m	=	Mass of the eVTOL aircraft
q	=	Dynamic pressure of the eVTOL aircraft

*Aerospace Engineer, Universities Space Research Association, NASA Ames Research Center, AIAA Member.
†Senior Scientist and Lead, Crown Consulting Inc., NASA Ames Research Center, AIAA Associate Fellow.
‡Senior Scientist, Universities Space Research Association, NASA Ames Research Center, AIAA Fellow.
§Senior Software Developer, Crown Consulting Inc., NASA Ames Research Center.
¶Aerospace Engineer, Aviation Systems Division, NASA Ames Research Center, AIAA Member.
‖Aerospace Research Engineer, Aviation Systems Division, NASA Ames Research Center, AIAA Associate Fellow.
**Aerospace Engineer, Aviation Systems Division, NASA Ames Research Center.
††Ames Associate, Aviation Systems Division, NASA Ames Research Center, AIAA Fellow.

ρ = Density of air
W_N = North component of wind velocity
W_E = East component of wind velocity
α = Angle of attack of air-stream relative to rotor tip path plane
ψ = Heading angle of the eVTOL aircraft
χ = Course angle of the eVTOL aircraft
θ = Rotor tip-path-plane pitch angle
ϕ = Rotor tip-path-plane roll angle
κ = Induced power factor
P_{max} = Total deliverable power
A_{rotor} = Rotor disk area
R = Radius of the rotor
R_{Earth} = Radius of the Earth assuming spherical model
Ω = Rotational velocity of the rotor blades
σ = Thrust weighted solidity ratio
$C_{\text{d mean}}$ = Mean blade drag coefficient

II. Introduction

Urban Air Mobility (UAM) can alleviate transportation congestion on the ground by utilizing three-dimensional (3D) airspace efficiently, just as skyscrapers allowed cities to use limited land more efficiently [1]. The envisioned concept of UAM involves a network of small electric aircraft that takeoff and land vertically (eVTOL) that can enable rapid and reliable transportation between suburbs and cities and, ultimately, within cities [1–4].

Recently, technological advances have made it possible to build and flight test eVTOL aircraft [2, 4, 5]. Several companies, for example, Airbus A^3, Aurora Flight Sciences, EHang, Joby Aviation, Kitty Hawk, Leonardo, Lilium, Terrafugia, and Volocopter, are pursuing different design approaches to make eVTOLs a reality [4]. Despite various designs, they all have distributed electric propulsion (DEP) systems in common [2]. However, the low specific energy of current lithium-ion polymer (Li-Po) battery technology used in DEP imposes constraints on the flight endurance of such aircraft. In general, multirotor eVTOLs are a relatively low cruise speed aircraft compared to winged eVTOL aircraft; therefore, atmospheric winds play a significant role in their trajectories. The operational benefits of wind-optimal trajectories have been extensively studied for commercial aircraft [6–8] but not for eVTOLs in the UAM environment. Therefore, in the current research, the operational benefits of wind-optimal trajectories are studied in the UAM context.

The focus of the current research is on the trajectories of a multirotor eVTOL aircraft on short UAM missions (less than 60 miles) [1, 9]. Therefore, an optimal control model for a multirotor eVTOL is formulated that includes a wind effect model to quantify the effect of wind on the trajectory. The optimal control problem, formulated using a lateral dynamics model and operational constraints, is numerically solved using the direct collocation method. The primary motivation of the paper is to determine if there is an operational benefit using wind-optimal trajectories for short flights (less than 60 miles) in the urban environment. Energy consumption and flight duration flying wind-optimal trajectories between origins and destinations in the Dallas-Fort Worth and New York metropolitan areas are compared with the corresponding energy consumption and flight duration flying on the great-circle paths between the same origin and destination pairs to determine the operational benefit of wind-optimal routing for short flights.

In this research, the concept of operations (CONOPs) of the multirotor eVTOL aircraft is assumed to be as follows: i) vertical climb; ii) cruise at a constant altitude along a path between UAM vertiports in metropolitan areas like the Dallas-Fort Worth and New York; and iii) vertical descent. The scope of this research is focused on the low-altitude (1600 ft above mean sea level (MSL)) cruise phase [10]; therefore, vertical climb and descent phases have been ignored in the problem formulation.

The rest of the paper is organized as follows: (i) In section III, the optimal control problem with energy consumption as the performance index is formulated to generate 4D trajectories for a multirotor eVTOL aircraft. The optimal control model presented includes a wind model for quantifying the effect of wind on a trajectory; (ii) In section IV, wind-optimal and great-circle trajectories are generated for the multirotor eVTOL in the Dallas-Fort Worth and New York metropolitan areas under different wind conditions using the direct method. The flight duration results for different scenarios are validated using a simulation tool designed and developed by NASA; and (iii) Finally, in section V, the main findings for this research study are summarized.

III. Optimal Control Model

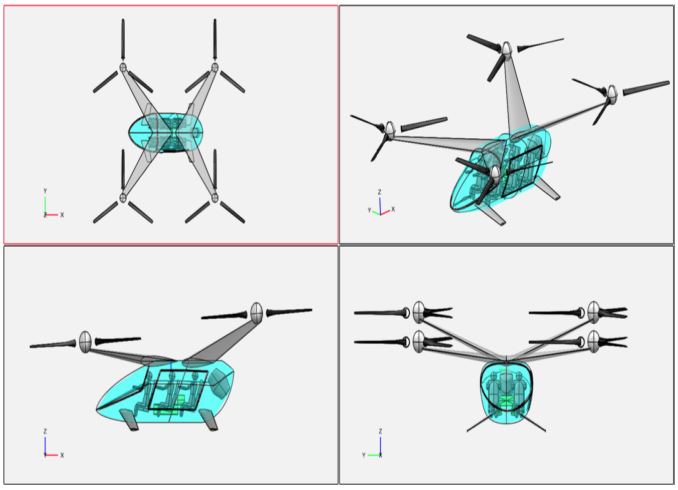

Fig. 1 Quadrotor eVTOL aircraft [11]

A. eVTOL Aircraft Model

In this research, a quadrotor eVTOL aircraft concept proposed by Silva et al. [11], as shown in Figure 1, is used to study the effect of wind on a multirotor eVTOL aircraft on UAM missions. The eVTOL has six-seater (up to 545 kg payload) capacity with the best range speed of 50.4 m/s (98 kts).

Table 1 shows performance data of the eVTOL aircraft [11] used in this research for trajectory optimization in cruise phase.

Table 1 Performance data of the eVTOL aircraft

Parameter (Unit)	Value
V_{cruise} (m/s)	50.41
R (m)	4.0
A_{rotor} (m^2)	50.26
mass (kg)	2940
σ	0.055
$C_{\text{d mean}}$	0.0089
F_{P}	0.97
κ	1.75
Ω (rad/sec)	30.12
P_{max} (kw)	494.25

B. Flight Dynamics and Kinematics Model

To study the effect of wind on the cruise phase of the multirotor eVTOL aircraft, a lateral flight dynamics model (two dimensional in space and one dimensional in time) is considered. The four lateral states of the model are: λ, τ, V, ψ; where λ is the latitude, τ is the longitude, V is the true airspeed (assumed to have only horizontal component during the cruise) and ψ is the heading angle w.r.t north [12, 13]. The three control variables of the model are: the net thrust (T), the rotor tip path plane pitch angle (θ) and the rotor tip path plane roll (bank) angle (ϕ). Therefore, the quasi-steady cruise flight dynamics and kinematics of the multirotor eVTOL aircraft under wind conditions in a vehicle carried frame of reference are as follows [2, 3, 8, 12–15]:

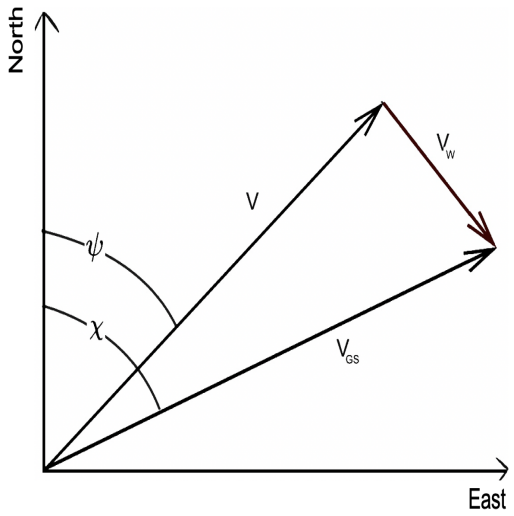

Fig. 2 Lateral navigation of an eVTOL aircraft

$$\frac{dV}{dt} = \frac{T\cos\phi\sin\theta - D}{m} - \frac{dW_N}{dt}\cos\psi - \frac{dW_E}{dt}\sin\psi \tag{1}$$

$$V\frac{d\psi}{dt} = \frac{T\sin\phi}{m} + \frac{dW_N}{dt}\sin\psi - \frac{dW_E}{dt}\cos\psi \tag{2}$$

$$(R_{\text{Earth}} + h)\frac{d\lambda}{dt} = V\cos\psi + W_N = V_{GS}\cos\chi \tag{3}$$

$$(R_{\text{Earth}} + h)\cos\lambda\frac{d\tau}{dt} = V\sin\psi + W_E = V_{GS}\sin\chi \tag{4}$$

where D is the parasite drag, V_{GS} is the ground speed, χ is the course, h is the altitude above mean sea level and R_{Earth} is the mean radius of the Earth and, W_N and W_E are the components of the wind in north and east directions, respectively. In this research, time derivative of wind components is assumed to be zero given the short range operations are expected to be less than 60 miles [1, 4].

For the quadrotor eVTOL aircraft, assuming that the rotors have negligible interference with each other, the net thrust (T) produced by the four rotors is given by:

$$T = \sum_{n=1}^{4}(T_{\text{rotor}})_n \tag{5}$$

where $(T_{\text{rotor}})_n$ is the thrust produced by the n^{th} rotor. Also, assuming all the rotors produce the same amount of thrust (T_{rotor}) in cruise phase, the net thrust (T) produced by the rotors is given by:

$$T = 4T_{\text{rotor}} \tag{6}$$

C. Drag Model

The parasite drag (D) on the multirotor eVTOL is calculated as follows [11]:

$$D = 1.1984q \tag{7}$$

where q is the dynamic pressure (N/m^2). The dynamic pressure (q) is calculated as follows:

$$q = \frac{\rho V^2}{2} \tag{8}$$

where ρ is the density of air, which is a function of altitude.

D. Momentum Theory in Hover

Using momentum theory [16–18], the hover induced velocity (v_h) is given by:

$$v_h = \sqrt{\frac{T_\mathrm{rotor}}{2\rho A_\mathrm{rotor}}} \tag{9}$$

where A_rotor is the rotor disk area (πR^2) and R is the radius of the rotor.

E. Momentum Theory in Forward Flight

Consider an isolated rotor in forward motion at true airspeed (V), with angle of attack (α) between the air-stream and the rotor disk (tip path plane). The solution for induced velocity (v_i) is given by [16–18]:

$$v_i = \frac{v_h^2}{\sqrt{(V\cos\alpha)^2 + (V\sin\alpha + v_i)^2}} \tag{10}$$

where the hover induced velocity (v_h) on the right-hand side of the equation (10) is computed using the equation (9).

The equation (10) is a quartic polynomial that can be analytically solved for induced velocity (v_i). Out of the four roots of the quartic equation (10), the one with real-positive and value lower than v_h is the correct solution for cruise phase. The equation (10) can also be numerically solved using an iterative technique with initial guess for v_i as v_h.

Once v_i is computed, the induced power loss of an isolated rotor ($P_\mathrm{induced\ rotor}$) in forward flight is computed as follows [18, 19]:

$$P_\mathrm{induced\ rotor} = \kappa T_\mathrm{rotor} v_i \tag{11}$$

where the induced power factor (κ) is assumed to be 1.75 in this research [11].

F. Power Required by the eVTOL Aircraft

Based on the quasi-steady flight assumption in the current research, the instantaneous power required in forward cruise flight at a constant altitude is equal to the sum of the induced power, parasite power, and profile power as follows [2, 3, 17, 18, 20]:

$$P_\mathrm{required} = P_\mathrm{induced} + P_\mathrm{parasite} + P_\mathrm{profile} \tag{12}$$

The induced power loss of the eVTOL aircraft (P_induced) is equal to the summation of the induced power loss of each rotor ($P_\mathrm{induced\ rotor}$). Therefore, the induced power loss of the quadrotor eVTOL aircraft is given by [11, 18]:

$$P_\mathrm{induced} = \sum_{n=1}^{4} (P_\mathrm{induced\ rotor})_n = \kappa \sum_{n=1}^{4} (T_\mathrm{rotor} v_i)_n \tag{13}$$

The power required to propel the eVTOL aircraft forward (the parasite power loss) at a constant altitude is given by [18]:

$$P_\mathrm{parasite} = TV\sin\alpha \tag{14}$$

The profile power loss is calculated from a mean blade drag coefficient ($C_\mathrm{d\ mean}$) as follows [11, 18, 21]:

$$P_\mathrm{profile} = \frac{\rho A_\mathrm{rotor} (\Omega R)^3 \sigma C_{d\ mean} F_P}{8} \tag{15}$$

where Ω is the rotational velocity of the rotor blades, σ is the thrust weighted solidity ratio, $C_\mathrm{d\ mean}$ is the mean blade drag coefficient and F_P is the function that accounts for the increase of the blade section velocity with rotor edgewise and axial speed [11, 18, 21]. However, F_P is assumed to be a constant (Table 1) in this research because of cruise at constant altitude and nominal cruise speed.

Therefore, using the equations from (12) to (15), the instantaneous power required (P_required) in forward flight is given by:

$$P_\mathrm{required} = \kappa \sum_{n=1}^{4} (T_\mathrm{rotor} v_i)_n + TV\sin\alpha + \frac{\rho A_\mathrm{rotor} (\Omega R)^3 \sigma C_{d\ mean} F_P}{8} \tag{16}$$

G. Performance Index of Optimal Control Problem

The performance index for the wind-optimal trajectory optimization problem is as follows:

$$J = \int_{t_0}^{t_f} (P_{\text{required}})dt = \int_{t_0}^{t_f} (\kappa \sum_{n=1}^{4} (T_{\text{rotor}} v_i)_n + TV \sin\alpha + \frac{\rho A_{\text{rotor}} (\Omega R)^3 \sigma C_{d\ mean} F_P}{8})dt \tag{17}$$

where t_0 is the initial flight time at the top of climb (TOC) placed directly above the origin vertiport at the cruise altitude and t_f is the final flight time to reach the top of descent (TOD) placed directly above the destination vertiport at the cruise altitude.

H. Path Constraints of Optimal Control Problem

For a level flight (cruise) in the presence of zero vertical wind, the net vertical force on the multirotor eVTOL aircraft is zero; therefore, the following path constraint is imposed on the problem:

$$T \cos\phi \cos\theta = mg \tag{18}$$

where m is the mass of the multirotor eVTOL aircraft and g is the acceleration due to the gravity.

The instantaneous power required (P_{required} in kw) is bounded by the total deliverable power (P_{max}) of the quadrotor eVTOL aircraft[11, 19]:

$$P_{\text{required}} \leq 494.25 \tag{19}$$

where P_{required} is defined in equation 16.

I. Great-Circle Path Constraint

The course angle (χ) for the great-circle trajectory between the two waypoints is calculated as follows [22]:

$$tan\chi = \frac{sin(\tau_2 - \tau_1)cos\lambda_2}{sin\lambda_2 cos\lambda_1 - sin\lambda_1 cos\lambda_2 cos(\tau_2 - \tau_1)} \tag{20}$$

where the origin latitude-longitude is (λ_1, τ_1) and the destination latitude-longitude is (λ_2, τ_2). However, to generate a great-circle trajectory between the two waypoints using the optimal control framework developed in this research, a path constraint as a function of the wind components (W_N and W_E), latitude-longitude coordinates of the two waypoints and heading angle (ψ) is required. Therefore, the course angle (χ) needs to be eliminated from the equation (20).

Using the equations (3) and (4), the heading angle (ψ) required to fly the course angle (χ) in the presence of the wind is computed as follows:

$$tan\chi = \frac{Vsin\psi + W_E}{Vcos\psi + W_N} \tag{21}$$

where W_N and W_E are the components of the wind in north and east directions respectively.

Given same left-hand side of the equations (20) and (21), therefore, the right-hand sides of the equations can be equated as follows:

$$\frac{Vsin\psi + W_E}{Vcos\psi + W_N} = \frac{sin(\tau_2 - \tau_1)cos\lambda_2}{sin\lambda_2 cos\lambda_1 - sin\lambda_1 cos\lambda_2 cos(\tau_2 - \tau_1)} \tag{22}$$

Hence, the path constraint for the great-circle trajectory between the two waypoints is given by:

$$(Vsin\psi + W_E)(sin\lambda_2 cos\lambda_1 - sin\lambda_1 cos\lambda_2 cos(\tau_2 - \tau_1)) - (Vcos\psi + W_N)(sin(\tau_2 - \tau_1)cos\lambda_2) = 0 \tag{23}$$

IV. Numerical Study and Results

A. Wind Data

The Rapid Refresh (RR) operational weather prediction system, available on an hourly basis at 13 km spatial resolution from the National Center for Environmental Prediction [23], has been used to extract the wind data for analysis. The wind data are extracted for January 2019 (i.e., 31 days) during peak traffic hours in the morning, i.e., 7 AM to 11 AM at cruise altitude (1600 ft above MSL) in 1-minute intervals at two major metropolitan areas (Dallas-Fort Worth and New York) of the United States. The extracted wind data are analyzed to find the date and local time when the wind magnitude is the highest (strongest wind) at these two metropolitan areas.

B. Optimal Control Solver

The trajectory optimization problems can be numerically solved, either using the direct or indirect method [24]. Direct methods typically discretize the trajectory optimization problem, and convert the original trajectory optimization problem into a non-linear program. On the other hand, indirect methods are characterized by explicitly solving the optimality conditions stated in terms of the adjoint differential equations, the maximum principle, and associated boundary (transversality) conditions [25]. Using the calculus of variations, the optimal control necessary conditions can be derived by setting the first variation of the Hamiltonian function to zero. A common way to distinguish these two methods is that a direct method discretizes and then optimizes, while an indirect method optimizes and then discretizes [24, 26].

In this research, PSOPT has been used to solve the optimal control problem to generate wind-optimal trajectories for the multirotor eVTOL aircraft. PSOPT is an open-source optimal control software package written in C++ that uses direct collocation methods such as pseudospectral methods [27]. Pseudospectral methods directly discretize the original optimal control problem to formulate a non-linear programming problem, which is then solved numerically using a sparse non-linear programming solver to find approximate local optimal solutions. IPOPT is an open-source C++ package for large-scale non-linear optimization, which uses an interior point method [27, 28]. IPOPT is the default non-linear programming algorithm used by PSOPT.

C. FACET

Future Air Traffic Management (ATM) Concepts Evaluation Tool (FACET) is a tool designed and developed by NASA over the last 20 years to provide a flexible simulation environment for the exploration, development and evaluation of advanced ATM concepts [29]. FACET models four-dimensional (4D) aircraft trajectories in the presence of winds using round-earth kinematic equations. Aircraft can be flown along flight plan routes or great-circle routes as they climb, cruise and descend per their aircraft-type performance models. Performance parameters of the aircraft are obtained from a data look-up table. Therefore, for the current research, a look-up table is created for the multirotor eVTOL aircraft based on the performance data of the conceptual multirotor eVTOL proposed by Silva, et al. [11]. In this research, the flight duration results of the optimal control framework using PSOPT solver are validated using the neighboring-optimal wind routing algorithm [30] implemented in FACET for computing the wind-optimal route. FACET implementation performs a bi-linear interpolation in spatial and temporal dimensions on the available gridded wind data.

D. Case Study - Dallas-Fort Worth Metropolitan Area

For the Dallas-Fort Worth metropolitan area, as stated earlier, the wind data are extracted at 1600 ft above MSL in 1-minute time intervals at grid points shown in Figure 3. The grid points are equispaced 10 km apart and cover 10^4 km^2 area.

To find the date and local time when the strongest wind (highest wind speed) occurred: First, the spatial average of wind speed is computed in 1-minute intervals (epochs). Second, the spatially averaged wind speeds at each epoch are compared to find the epoch at which the highest wind speed occurred. The data analytics results showed that the strongest wind (maximum wind speed) occurred on January 19, 2019, at 8 AM Central Standard Time (CST) i.e., at epoch = 1547906400 seconds. The statistics of the wind data on January 19, 2019, at 8 AM in the Dallas-Fort Worth metropolitan area are shown in Table 2.

To solve for the wind-optimal trajectories in the Dallas-Fort Worth metropolitan area using the optimal control

Table 2 Statistics of wind in the Dallas-Fort Worth metropolitan area on January 19, 2019, at 8 AM CST

	North Wind (W_N m/s)	East Wind (W_E m/s)	Wind Speed (V_W in m/s)
Spatial Average	-16.92	10.83	20.08
Standard Deviation	0.27	0.25	0.26

solver PSOPT, the north and the east components of the wind are assumed to be uniform in the chosen region, given the relatively small standard deviations of wind components as shown in Table 2. Therefore, the north component of the wind (W_N in m/s) and the east component of the wind (W_E in m/s) are modeled as follows in the Dallas-Fort Worth metropolitan area:

$$W_N = -16.92 \tag{24}$$

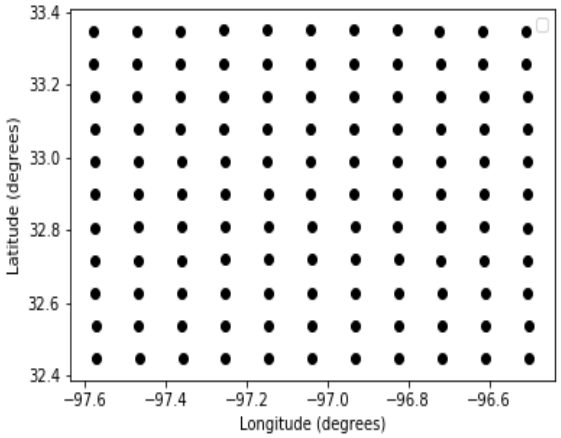

(a) Grid points to extract wind data

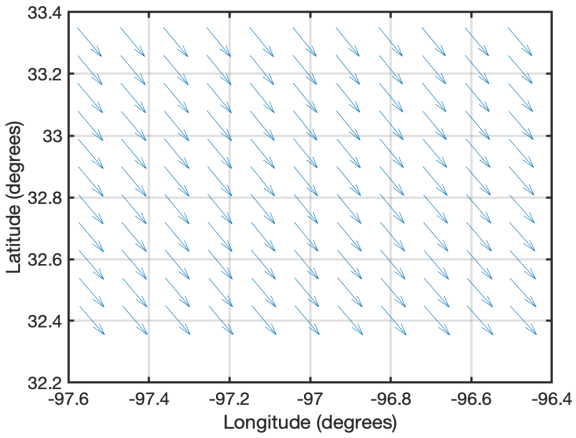

(b) Wind field at epoch = 1547906400 (seconds)

Fig. 3 Wind data extracted at equispaced grid points in the Dallas-Fort Worth metropolitan area

$$W_E = 10.83 \tag{25}$$

To study wind-optimal trajectories, three routes originating from the vertiport at KKEG (32.901767, -97.193954), are considered. Based on the longest great-circle distance between the vertiports in UAM - X2 engineering evaluation [10], the destination vertiports are chosen 30 nautical miles from the origin. The destinations (as shown in Table 3) are also chosen such that the initial bearing of the great-circle routes approximately faces crosswind, headwind, and tailwind, respectively.

Table 3 Locations of origin and destination of routes in the Dallas-Fort Worth metropolitan area

Scenario	Origin (Latitude, Longitude)	Destination (Latitude, Longitude)
Crosswind	(32.901767, -97.193954)	(33.170832, -96.692252)
Headwind	(32.901767, -97.193954)	(33.323242, -97.515717)
Tailwind	(32.901767, -97.193954)	(32.479399, -96.875310)

From Figure 4, it can be seen that in the uniform wind field, for the multirotor eVTOL aircraft on a short UAM mission (30 nm), the energy consumption and flight duration for the wind-optimal trajectories are same as the corresponding great-circle trajectories. However, because of the slow nominal cruise speed (50.41 m/s), the energy consumption and flight duration while flying in the headwind is 2-3 times higher than flying the same distance (30 nm) in the tailwind. As shown in Figure 4, the flight duration (cruise) results of PSOPT are validated using overall flight duration (climb, cruise and descent) results of FACET. The flight duration results of FACET are in general slightly higher (1 - 2 mins) because of the short climb and descent phases.

E. Case Study - New York Metropolitan Area

Similar to the Dallas-Fort Worth case study, wind data are sampled at the 1-minute interval at grid locations 10 km apart in the New York metropolitan area, as shown in Figure 5a. Following the earlier process, the maximum value of the wind speed occurred on January 24, 2019, at 10 AM Eastern Standard Time (EST) i.e., at epoch = 1548342000 (seconds); Figure 5b shows the corresponding wind field. The statistics of the wind data are shown in Table 4.

Because PSOPT requires the equations in an analytical form, the MATLAB curve-fitting toolbox [31] is used for obtaining equations for north and east components of the wind, needed in equations (3) and (4). This resulted in the following wind model:

$$W_N = 1218 - 691.3\lambda + 539.4\tau \tag{26}$$

$$W_E = 380 - 253.5\lambda + 153.9\tau \tag{27}$$

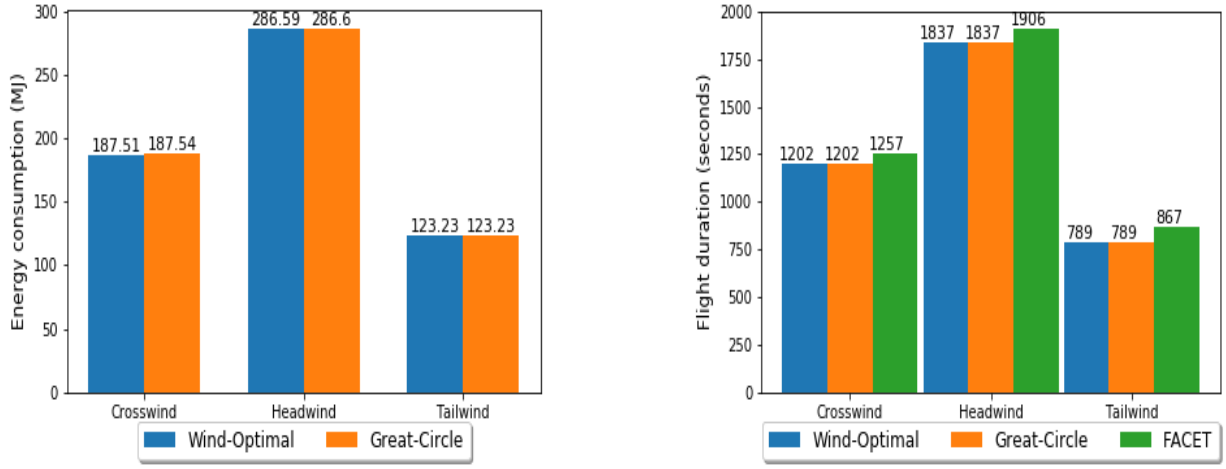

(a) Energy consumption (MJ)

(b) Flight duration (seconds)

Fig. 4 Comparison of wind-optimal and great-circle trajectories under different wind conditions in the Dallas-Fort Worth metropolitan area

Table 4 Statistics of wind in the New York metropolitan area on January 24, 2019, at 10 AM EST

	North Wind (W_N m/s)	East Wind (W_E m/s)	Wind Speed (V_W in m/s)
Spatial Average	28.35	0.54	28.40
Standard Deviation	5.01	1.67	5.02

where λ (rad) is the latitude and and τ (rad) is the longitude. The R-square values of the obtained equations: (26) and (27), are 0.9764 and 0.9441 respectively. Figures 6a and 6b show the fitted surfaces described by the equations (26) and (27).

To study wind-optimal trajectories, three routes originating from the vertiport at KEWR (40.703869, -74.176071) are considered. Based on the longest great-circle distance between the vertiports in UAM - X2 engineering evaluation [10], the destination vertiports are chosen 30 nautical miles from the vertiport at KEWR in the New York metropolitan area. The destinations (as shown in Table 5) are also chosen such that the initial bearing of the great-circle routes approximately faces crosswind, headwind, and tailwind, respectively.

From Figure 7, it can be seen that in the non-uniform wind field, the energy consumption and flight duration for the

Table 5 Locations of origin and destination of routes in the New York metropolitan area

Scenario	Origin (Latitude, Longitude)	Destination (Latitude, Longitude)
Crosswind	(40.703869, -74.176071)	(40.701997, -73.518651)
Headwind	(40.703869, -74.176071)	(40.203523, -74.176071)
Tailwind	(40.703869, -74.176071)	(41.204171, -74.176071)

wind-optimal trajectory are 1.2 % lower than the corresponding great-circle trajectory. However, because of the slow nominal cruise speed (50.41 m/s) and high magnitude of the headwind (approx. 28 m/s), the energy consumption and flight duration while flying in the headwind are 4-5 times higher than flying the same distance (30 nm) in the tailwind. As shown in Figure 7, the flight duration (cruise) results of PSOPT are validated using overall flight duration (climb, cruise and descent) results of FACET. The flight duration results of FACET are in general slightly higher (1 - 2 mins) because of the short climb and descent phases.

To perform the sensitivity analysis on wind-optimal trajectory, the headwind route is further extended to 50 nm

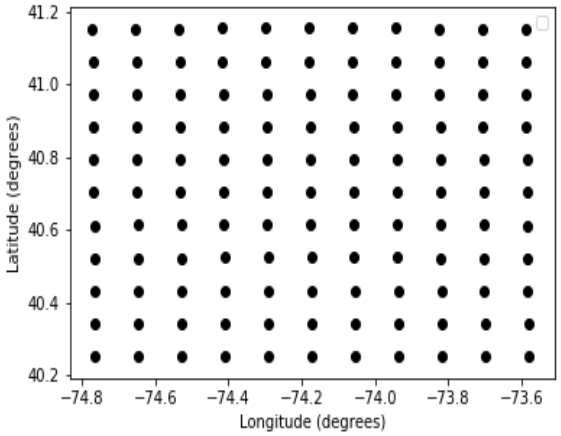

(a) Grid points to extract wind data

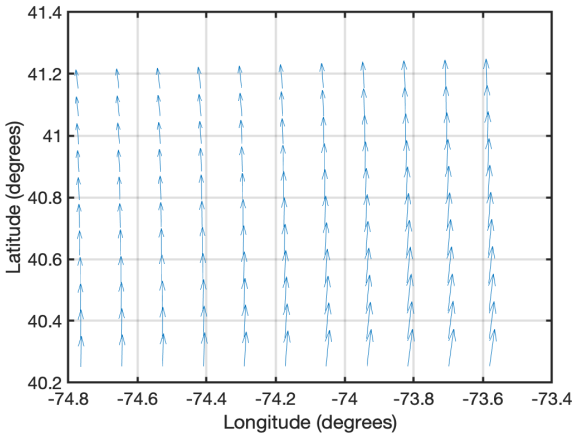

(b) Wind field at epoch = 1548342000 (seconds)

Fig. 5 Wind data extracted at equispaced grid points in the New York metropolitan area

(57.54 miles). The headwind route is picked among the three routes because it showed the greatest operational benefit (1.2 %) for wind-optimal trajectory when compared to the corresponding great-circle trajectory. For the headwind route (origin: 41.3661, -74.176071 and destination: 40.2, -74.176071), the operational benefits with the wind-optimal trajectory when compared to the great-circle trajectory are less than 2.5 % as shown in Table 6.

Table 6 Comparison of wind-optimal trajectory with great-circle trajectory on headwind route (50 nm)

Trajectory type	Energy consumption (MJ)	Flight duration (seconds)
Wind-Optimal	629.88	4037.71
Great-Circle	646.45	4143.9

F. Case Study - Simulated Wind in the Dallas-Fort Worth Metropolitan Area

To study the impact of wind field with varying direction on wind-optimal trajectories, a wind field is simulated such that the north component of the wind (W_N) is linearly varied from + 15 m/s at the origin vertiport (32.901767, -97.193954) to - 15 m/s at the destination vertiport (32.897850, -96.204208) as shown in Figure 8.

The linear curve-fit of the north component of the wind (W_N in m/s) obtained using the MATLAB curve-fitting tool [31] is as follows:

$$W_N = -1736.68\tau - 2931.03 \tag{28}$$

$$W_E = 15 \tag{29}$$

From Table 7, it can be seen that in the wind field with varying direction as shown in Figure 8, for the multirotor

Table 7 Comparison of wind-optimal trajectory with great-circle trajectory in simulated wind with varying direction

Trajectory type	Energy consumption (MJ)	Flight duration (seconds)
Wind-Optimal	220.54	1413.76
Great-Circle	223.12	1430.02

eVTOL aircraft on a short UAM mission (30 nm), the energy consumption and flight duration for the wind-optimal trajectory are approximately 1.4 % lower than the corresponding great-circle trajectory (Figure 9).

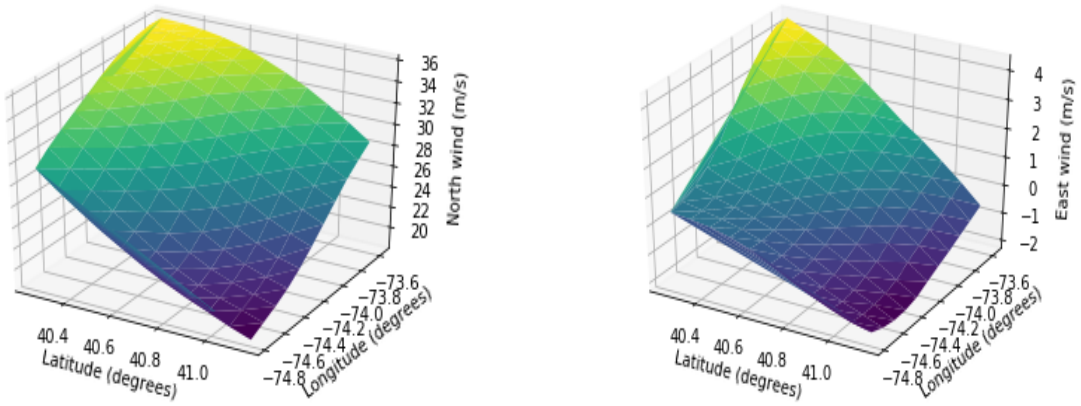

(a) North wind component (W_N)

(b) East wind component (W_E)

Fig. 6 Wind surface map in the New York metropolitan area on January 24, 2019, at 10 AM EST

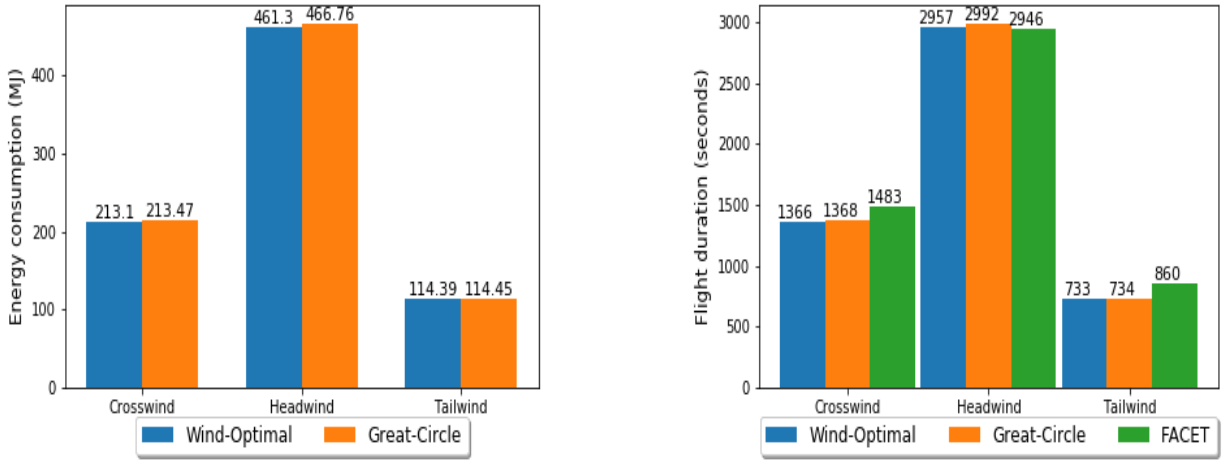

(a) Energy consumption (MJ)

(b) Flight duration (seconds)

Fig. 7 Comparison of wind-optimal and great-circle trajectories under different wind conditions in the New York metropolitan area

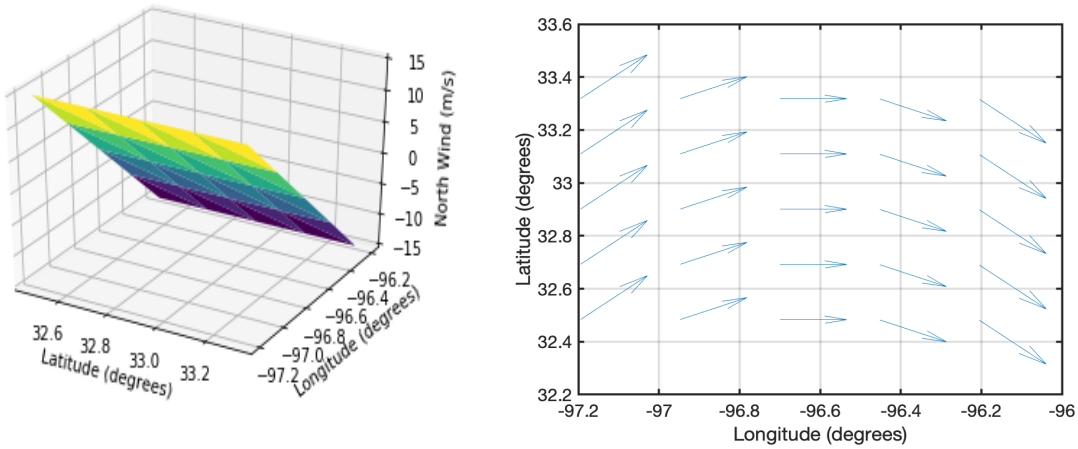

(a) Surface map of simulated north wind (W_N in m/s)

(b) Simulated wind field (varying direction)

Fig. 8 Wind field with varying direction to study wind-optimal trajectory in the UAM environment

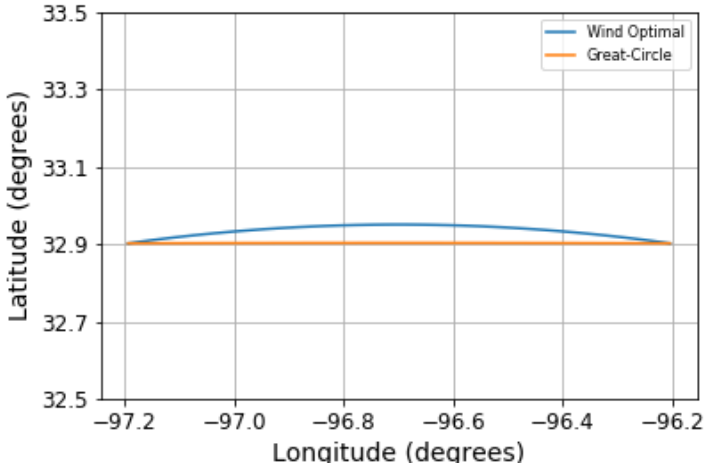

Fig. 9 Wind-optimal trajectory and great-circle trajectory in simulated wind with varying direction

V. Conclusion

In this research, the optimal control problem with energy consumption as the performance index is formulated to generate trajectories for a multirotor electric vertical takeoff and landing aircraft on a short urban air mobility mission (less than 60 miles). The optimal control model presented includes a wind model for quantifying the effect of wind on a trajectory. To create a wind model, for the Dallas-Fort Worth and New York metropolitan areas, the real wind data from the Rapid Refresh are used. Wind data are then analyzed to find the date and local time when the wind magnitude is the highest (strongest wind) at these two metropolitan areas. Finally, the wind models are created at these two metropolitan areas by performing a linear curve fit on the strongest wind data.

Further, this paper presents a framework to compare energy consumption and flight duration flying wind-optimal trajectories and great-circle trajectories to evaluate the operational benefit of wind-optimal routing for short flights. The formulated lateral trajectory optimization problem is numerically solved using the pseudospectral method for a NASA-proposed conceptual multirotor electric vertical takeoff and landing aircraft.

The numerical results in the Dallas-Fort Worth metropolitan area in the presence of uniform wind conditions suggest that wind-optimal trajectories are identical to the corresponding great-circle trajectories for short flights (30 nm). The numerical results in the New York metropolitan area in the presence of non-uniform wind conditions suggest that wind-optimal trajectories show slight operational benefits compared to the corresponding great-circle trajectories for short flights (30 nm) with maximum benefit (1.2 %) in the headwind condition. Upon performing a sensitivity analysis by extending the headwind route to 50 nm, the operational benefit increased to 2.4 %. The flight duration results for different scenarios are validated using a simulation tool designed and developed by NASA over the last 20 years for exploring advanced air traffic management concepts.

To substantiate the wind effect results from the New York metropolitan area, a simulated wind field was created such that the crosswind component of the wind to the direct route between origin and destination changes the direction completely, whereas the tailwind component remains constant. Under such wind conditions, the trajectory optimization results show the maximum operational benefit to be 1.4 %.

In conclusion, this research study suggests that for short flights in an urban environment, the wind-optimal trajectories have a very slight (insignificant) operational advantage over the great-circle trajectories in terms of energy consumption and flight duration. As expected, headwinds and tailwinds along the route of flight have a significant impact on energy consumption and flight duration.

Acknowledgments

The authors would like to thank Dr. Wayne Johnson, Christopher Silva, Carlos A. Malpica, and Dr. Gloria K.Yamauchi from Aeromechanics branch at NASA Ames Research Center, for constructive discussions and their valuable time. Also, special thanks to Christopher Silva for reviewing the drag and power equations.

References

[1] Uber-Elevate, "Fast-forwarding to the future of on-demand, urban air transportation," `https://www.uber.com/`, 2019. [Online; accessed 19-June-2019].

[2] Pradeep, P., and Wei, P., "Energy-Efficient Arrival with RTA Constraint for Multirotor eVTOL in Urban Air Mobility," *Journal of Aerospace Information Systems*, Vol. 16, No. 7, 2019, pp. 263–277. doi:10.2514/1.I010710.

[3] Pradeep, P., "Arrival management for eVTOL aircraft in on-demand urban air mobility," Ph.D. thesis, Iowa State University, Ames, 2019.

[4] Thipphavong, D. P., Apaza, R., Barmore, B., Battiste, V., Burian, B., Dao, Q., Feary, M., Go, S., Goodrich, H. J., Kenneth H, Idris, H. R., Kopardekar, P. H., Lachter, J. B., Neogi, N. A., Ng, H. K., Oseguera-Lohr, R. M., Patterson, M. D., and Verma, S. A., "Urban air mobility airspace integration concepts and considerations," *2018 Aviation Technology, Integration, and Operations Conference*, 2018, p. 3676. doi:10.2514/6.2018-3676.

[5] Bosson, C., and Lauderdale, T. A., "Simulation evaluations of an autonomous urban air mobility network management and separation service," *2018 Aviation Technology, Integration, and Operations Conference*, 2018, p. 3365. doi:10.2514/6.2018-3365.

[6] Sridhar, B., Ng, H. K., Linke, F., and Chen, N. Y., "Benefits analysis of wind-optimal operations for trans-atlantic flights," *14th AIAA Aviation Technology, Integration, and Operations Conference*, 2014, p. 2583.

[7] Ng, H. K., Sridhar, B., and Grabbe, S., "A practical approach for optimizing aircraft trajectories in winds," *2012 IEEE/AIAA 31st Digital Avionics Systems Conference (DASC)*, IEEE, 2012, pp. 3D6–1.

[8] Sridhar, B., Chen, N. Y., Hok, K. N., Rodionova, O., Delahaye, D., and Linke, F., "Strategic planning of efficient oceanic flights," *11th USA/Europe Air Traffic Management Research and Development Seminar June 23-26, 2015 Lisbon, Portugal*, 2015.

[9] "Uber Air Vehicle Requirements and Missions," , 2020. URL `https://s3.amazonaws.com/uber-static/elevate/SummaryMissionandRequirements.pdf`, [Online; accessed 16-April-2020].

[10] Verma, S. A., Monheim, S. C., Moolchandani, K. A., Pradeep, P., Cheng, A. W., Dulchinos, V. L., Dao, Q. V., Arneson, H. M., Lauderdale, T. A., and Thipphavong, D. P., "Lessons Learned: Using UTM paradigm for Urban Air Mobility operations," *Aviation 2020 Conference*, 2020. Submitted.

[11] Silva, C., Johnson, W. R., Solis, E., Patterson, M. D., and Antcliff, K. R., "VTOL Urban Air Mobility Concept Vehicles for Technology Development," *2018 Aviation Technology, Integration, and Operations Conference*, 2018, p. 3847.

[12] Yomchinda, T., Horn, J., and Langelaan, J., "Flight path planning for descent-phase helicopter autorotation," *AIAA Guidance, Navigation, and Control Conference*, 2011, p. 6601.

[13] Tsuchiya, T., Ishii, H., Uchida, J., Ikaida, H., Gomi, H., Matayoshi, N., and Okuno, Y., "Flight trajectory optimization to minimize ground noise in helicopter landing approach," *Journal of guidance, control, and dynamics*, Vol. 32, No. 2, 2009, pp. 605–615.

[14] Weitz, L. A., "Derivation of a point-mass aircraft model used for fast-time simulation," *MITRE Corporation*, 2015.

[15] Erzberger, H., and Lee, H., "Constrained optimum trajectories with specified range," *Journal of Guidance and Control*, Vol. 3, No. 1, 1980, pp. 78–85.

[16] Hoffmann, G., Huang, H., Waslander, S., and Tomlin, C., "Quadrotor helicopter flight dynamics and control: Theory and experiment," *AIAA Guidance, Navigation and Control Conference and Exhibit*, 2007, p. 6461.

[17] Heyson, H. H., "A momentum analysis of helicopters and autogyros in inclined descent, with comments on operational restrictions," 1975.

[18] Johnson, W., *Helicopter theory*, Courier Corporation, 2012.

[19] Johnson, W., "NDARC-NASA Design and Analysis of Rotorcraft," 2015.

[20] Leishman, J., *Principles of helicopter aerodynamics*, Cambridge Aerospace Series, Cambridge University Press, 2002. URL `https://books.google.com/books?id=-PnV2JuLZi4C`.

[21] Johnson, W., Silva, C., and Solis, E., "Concept Vehicles for VTOL Air Taxi Operations," *Conference on Aeromechanics Design for Transformative Vertical Flight, San Francisco, CA*, 2018.

[22] Chatterji, G., Sridhar, B., and Bilimoria, K., "En-route flight trajectory prediction for conflict avoidance and traffic management," *Guidance, Navigation, and Control Conference*, 1996, p. 3766.

[23] Benjamin, S. G., Brown, J. M., Brundage, K. J., Schwartz, B. E., Smirnova, T. G., Smith, T. L., and Morone, L. L., "NWS Technical Procedures Bulletin 448 RUC-2-The Rapid Update Cycle Version 2," 1998.

[24] Betts, J. T., and Huffman, W. P., "Mesh refinement in direct transcription methods for optimal control," *Optimal Control Applications and Methods*, Vol. 19, No. 1, 1998, pp. 1–21.

[25] Bryson, A. E., *Applied optimal control: optimization, estimation and control*, CRC Press, 1975.

[26] Kelly, M., "An introduction to trajectory optimization: How to do your own direct collocation," *SIAM Review*, Vol. 59, No. 4, 2017, pp. 849–904.

[27] Becerra, V. M., "Solving complex optimal control problems at no cost with PSOPT," *2010 IEEE International Symposium on Computer-Aided Control System Design*, 2010, pp. 1391–1396. doi:10.1109/CACSD.2010.5612676.

[28] Wächter, A., and Biegler, L. T., "On the implementation of an interior-point filter line-search algorithm for large-scale nonlinear programming," *Mathematical programming*, Vol. 106, No. 1, 2006, pp. 25–57. doi:10.1007/s10107-004-0559-y.

[29] Bilimoria, K. D., Sridhar, B., Grabbe, S. R., Chatterji, G. B., and Sheth, K. S., "FACET: Future ATM concepts evaluation tool," *Air Traffic Control Quarterly*, Vol. 9, No. 1, 2001, pp. 1–20.

[30] Jardin, M. R., and Bryson Jr, A. E., "Neighboring optimal aircraft guidance in winds," *Journal of Guidance, Control, and Dynamics*, Vol. 24, No. 4, 2001, pp. 710–715.

[31] Toolbox, C. F., "For Use with MATLAB;[user's Guide]," *Natick, MA: MathWorks*, 2001.